

## Ozone Production from the 2004 North American Boreal Fires

G.G. Pfister<sup>1</sup>, L.K. Emmons<sup>1</sup>, P.G. Hess<sup>1</sup>, R. Honrath<sup>2</sup>, J.-F. Lamarque<sup>1</sup>, M. Val Martin<sup>2</sup>,  
R.C. Owen<sup>2</sup>, M.A. Avery<sup>3</sup>, E.V. Browell<sup>3</sup>, J.S. Holloway<sup>4</sup>, P. Nedelec<sup>5</sup>, R. Purvis<sup>6</sup>, T.B  
Ryerson<sup>4</sup>, G.W. Sachse<sup>3</sup>, H. Schlager<sup>7</sup>

<sup>1</sup> *National Center for Atmospheric Research, Boulder, CO*

<sup>2</sup> *Michigan Technological University, Houghton, MI*

<sup>3</sup> *NASA Langley Research Center, Hampton, VA*

<sup>4</sup> *National Oceanic and Atmospheric Administration, Boulder, CO*

<sup>5</sup> *Centre National de la Recherche Scientifique, Toulouse, France*

<sup>6</sup> *Facility for Airborne Atmospheric Measurements, Cranfield, UK*

<sup>7</sup> *German Aerospace Center, Oberpfaffenhofen, Germany*

### Abstract

This paper examines the ozone production from boreal forest fires based on a case study of wildfires in Alaska and Canada in summer 2004. The model simulations were performed with the chemistry transport model MOZART-4 and were evaluated by comparison with a comprehensive set of aircraft measurements. In the analysis we use measurements and model simulations of carbon monoxide (CO) and ozone (O<sub>3</sub>) at the PICO-NARE station located in the Azores within the pathway of North American outflow. The modeled mixing ratios were used to test the robustness of the enhancement ratio  $\Delta O_3/\Delta CO$  (defined as the excess ozone mixing ratio normalized by the increase in CO) and the feasibility for using this ratio in estimating the ozone production from the

wildfires. Modeled and observed enhancement ratios are about 0.25 ppbv/ppbv which is in the range of values found in the literature, and results in a global net ozone production of  $12.9 \pm 2$  Tg O<sub>3</sub> during summer 2004. This matches the net ozone production calculated in the model for a region ranging from Alaska to the East Atlantic (9–11 Tg O<sub>3</sub>) indicating that observations at PICO-NARE representing photochemically well-aged plumes provide a good measure of the ozone production of North American boreal fires. However, net chemical loss of fire related ozone dominates in regions far downwind from the fires (e.g. Europe and Asia) resulting in a global net ozone production of 6 Tg O<sub>3</sub> during the same time period. On average, the fires increased the ozone burden (surface–300 mbar) over Alaska and Canada during summer 2004 by about 7–9%, and over Europe by about 2–3%. The disturbance in the ozone burden is a combination of ozone production from fire emissions and increased destruction of non-fire related ozone as indicated by analysis of ozone and CO fire tracers incorporated into the model simulations.

## 1 Introduction

Ozone (O<sub>3</sub>) plays a central role in tropospheric chemistry as a primary source of hydroxyl radicals and, by being toxic in nature, causes impacts on human and plant health. It is also estimated to be the third most important greenhouse gas [*Houghton et al.*, 2001]. The production of tropospheric ozone in the Northern mid-latitudes is largely impacted by anthropogenic sources [*Chandra et al.*, 2004]. Significant ozone enhancements have been observed in individual plumes of boreal forest fires [*Forster et al.*, 2001; *McKeen et al.*, 2002], but the large-scale impacts of high latitude biomass burning on the tropospheric ozone budget are poorly quantified. Measurements of ozone in the free troposphere in combination with global chemical transport models can help estimating the hemispheric impact of boreal fire emissions on tropospheric ozone.

Ozone is produced from anthropogenic and biomass burning sources when carbon monoxide (CO) or volatile organic compounds (VOCs) react with hydroxyl radicals in the presence of nitrogen oxides (NO<sub>x</sub>) and sunlight. CO is a long-lived tracer, and the relationship between mixing ratios of ozone and CO in transported regional plumes can be used as an indicator for the magnitude of net ozone production from selected sources.

It has been found that the enhancement ratio ( $\Delta\text{O}_3/\Delta\text{CO}$ ), given as the excess O<sub>3</sub> mixing ratio normalized by the increase in CO, is typically smaller for boreal forest fires than for tropical biomass and savannah burning or urban and industrial plumes, due to a lower NO<sub>x</sub>:CO emission ratio in boreal forest fires compared to the other sources [e.g. *Andreae et al.*, 1994; *Wofsy et al.*, 1992].  $\Delta\text{O}_3/\Delta\text{CO}$  of fire plumes is also expected to change with plume age. For example, *Yokelson et al.* [2003] found an increase from 0.09 ppbv/ppbv in

fresh tropical biomass burning plumes to 0.22 ppbv/ppbv for plumes 2–4 days old. Thus, ozone production downwind from the source region must be accounted for.

In this study we used a combination of model studies and observations to investigate the ozone production related to emissions from boreal forest fires. We focused our analysis on the wildfires that burned in Alaska and Canada in summer 2004 as these were the largest on record for Alaska. The CO emissions from these North American boreal fires have been estimated as  $30 \pm 5$  Tg for June through August [Pfister *et al.*, 2005]. A total of about 11 million acres were burned in Alaska and Canada during that time period.

The structure of this paper is the following. After the Introduction we discuss the model simulations and model evaluation in Sections 2 and 3, respectively. In Section 4 we describe CO and O<sub>3</sub> in-situ measurements taken at the PICO-NARE station located in the Azores. These observations were used in combination with model simulations to investigate the ozone production from the fires in Alaska and Canada in summer 2004. Section 5 discusses and evaluates different techniques for calculating the enhancement ratio and analyzes the ozone production due to emissions from the fires. The analysis is supported by incorporating fire tracers for CO and ozone into the model and by performing model simulations with and without fire emissions. Finally, we investigate the contributions these fires had on the Northern Hemispheric and regional budgets of CO and ozone. Section 6 summarizes our findings.

## 2 Model Simulation

The Model for OZone And Related chemical Tracers (MOZART) chemistry transport model has been developed at the National Center for Atmospheric Research, the Geophysical Fluid Dynamics Laboratory and the Max-Planck Institute for Meteorology. In this study we are using Version 4 [Emmons *et al.*, Sensitivity of chemical budgets to meteorology in MOZART-4, in preparation]. Modifications from Version 2 published in Horowitz *et al.* [2003] include, amongst others, a more complete description of anthropogenic hydrocarbon chemistry, the inclusion of tropospheric aerosols, and on-line calculations of dry deposition, H<sub>2</sub>O, and biogenic emissions.

We run the model at a horizontal resolution of ~2.8 degrees by 2.8 degrees. The meteorological fields for driving MOZART were taken from the National Centers for Environmental Prediction (NCEP) National Center for Atmospheric Research Re-Analysis [Kistler *et al.*, 2001] and were interpolated from a 6-hour time resolution to the 20-minute time steps of the simulations. The vertical resolution of the meteorological fields and hence the model consists of 28 hybrid levels ranging from the surface up to 2 hPa.

Biofuel and fossil fuel emissions used in this study were taken from the EU project POET [Granier *et al.*, 2004]. Over the continental US, the anthropogenic emissions are based on the U.S. EPA NEI-99 inventory (National Emissions Inventory, base year 1999, version 3) [EPA, 2004]. For the Alaska and Canada region, the biomass burning emissions for CO for 2004 were taken from an inverse modeling study [Pfister *et al.*, 2005], and emissions for NO<sub>x</sub> and VOCs were deduced from this inventory by applying emission

factors based on *Andreae and Merlet* [2001]. At the time these simulations were run, an emissions inventory for the year 2004 for biomass burning sources outside North America was not available. A comparison of CO data from the Measurements Of Pollution In The Troposphere (MOPITT) remote sensing instrument for 2000 – 2004 showed that the global biomass burning activity in summer 2004 was similar to 2002 and for this reason we used a 2002 biomass burning inventory based on ATSR fire counts [*Granier et al.*, 2004].

Our model simulations cover the months from June through August 2004 with a spin-up phase beginning in August 2003. We performed three different simulations. Two of these include emissions from the Alaskan and Canadian wildfires, and are abbreviated as *BB* in the following. In one of these simulations (*BBsurf*), the wildfire emissions were released at the lowest model layer and distributed in the boundary layer by the model boundary layer scheme. In the other simulation (*BBvert*), the emissions were distributed evenly with regard to number density between the surface and 9 km altitude to consider the effects of rapid vertical transport in fire-induced convective clouds. The 9 km altitude represents an upper limit for the injection height based on estimates derived from the Multi-Angle Imaging Spectro-Radiometer (MISR) and the Moderate Resolution Imaging Spectro-Radiometer (MODIS) [*Averill et al.*, 2005]. In a third simulation (*noBB*) used as a reference, the emissions of the wildfires in Alaska and Canada were set to zero.

We included two fire tracers in the model. Tracers are emitted or produced from a specific source, but undergo the same transport, chemistry, and physical processes as the standard species. The first tracer incorporated into the simulations is a CO fire tracer (*CO<sub>f</sub>*), i.e. CO released from the Alaska/Canada wildfires. For the second tracer we

tagged the ozone production resulting from hydrocarbon or CO oxidation in association with the emissions of  $\text{NO}_x$  from the fires. We refer to this tracer as  $O_3^{\text{NO}_x}$  in the following. The tagging technique for  $O_3^{\text{NO}_x}$  takes into account the re-cycling of  $\text{NO}_x$  from reservoirs such as PAN by applying tags to all nitrogen-containing species. Although there are some minor pathways to create ozone without the presence of  $\text{NO}_x$ , the accuracy of the tagging technique has been estimated as better than 95% on a monthly basis [Lamarque *et al.*, 2005]. The statistical analysis we perform using  $O_3^{\text{NO}_x}$  in this study is expected to give a comparable accuracy.

### 3 Model Evaluation

The model simulations have been evaluated by comparison with aircraft measurements taken in the framework of the ICARTT (International Consortium for Atmospheric Research on Transport and Transformation) campaign during summer 2004. Table 1 includes a list of the platforms, instrumentation, and corresponding references. Measurements with the NASA DC-8 covered large parts of North America and the Northern Atlantic, the NOAA-P3 flights were focused on the Eastern United States, the British BAE146 performed most flights over the Atlantic, and the German Falcon covered mostly Europe. The Measurements of OZone aboard Airbus In-service airCRAFT (MOZAIC) data set has global coverage, but we are including only measurements over North America, the Northern Atlantic and Europe in accordance with the regions covered by the other aircraft. Most low altitude measurements for this data set are from take-offs and landings over airports in Europe and the US. For a more detailed description of all flight patterns we refer to *Fehsenfeld et al.* [International Consortium for Atmospheric Research on Transport and Transformation (ICARTT): North America to Europe: Overview of the 2004 summer field study, submitted to *J. Geophys. Res.*, 2006].

For the comparison of the model with the observations, 2-hour average model data have been linearly interpolated to the time and location of the aircraft data. The time resolution of the observations is 1 minute. Statistics have been calculated for the individual aircraft data sets and binned onto a 2-km wide altitude grid. The results for *BBvert*, *BBsrf* and, for comparison, *noBB*, are shown in Figure 1 for CO and in Figure 2 for ozone, respectively. The agreement for CO as well as ozone is generally better in the simulations with fires

than in the simulation without fires. A clear change in the CO and O<sub>3</sub> mixing ratios between *BB* and *noBB* is seen in all data sets, also for the UK BAE146 and the DLR Falcon indicating that plumes from the Alaska and Canada fires reached all the way to Europe. In Table 2 we list statistics for modeled CO and O<sub>3</sub> concentrations for the different platforms. The altitude range considered spans from the surface to 8 km corresponds to the data sets shown in Figures 1 and 2. The T-test significance levels for simulations with and without fire emissions are above 99% for all platforms indicating the samples have significantly different means. It is interesting to note that O<sub>3</sub> mixing ratios from *BBvert* and *BBsrf* show significant difference in their means, while no significant difference is found for corresponding CO concentrations. This suggests ozone production from the fires was slightly more sensitive to the injection height than the concentration fields of CO.

For most altitudes and platforms, the CO bias between model and observations is less than 10% for both *BBsrf* and *BBvert* (see Figure 1). The mean bias as well as the correlation improved upon adding fire emissions into the model, with the only exception being the highest altitude bin for the NOAA P3 and DLR Falcon data set. The comparison for ozone (Figure 2) shows an agreement of better than 10% for all platforms and altitude bins when fire emissions are included in the simulations. In the lowest altitude level a positive ozone bias shows up over the US, though the reasons for this are not well understood. No clear conclusion can be drawn from the evaluation if either *BBsrf* or *BBvert* lead to better agreement. The fires in Alaska and Canada were a combination of crown, smoldering, and peat fires, and the two cases we ran do not

represent the full complexity of fire behavior, but are probably better regarded as sensitivity tests to the vertical distribution of emissions.

## 4 CO and O<sub>3</sub> at PICO-NARE

### 4.1 Observations

For the analysis of the ozone production from the wildfires in Alaska and Canada we made use of in-situ measurements at the PICO-NARE station. The station is located on the summit caldera of Pico mountain on Pico Island in the Azores, Portugal (2225 m above sea level, 38.47N, 28.40W) and is well suited for studying North American pollution outflow. Air masses at this location typically arrive from North America, but frequently originate from high latitude regions such as Alaska and Siberia [*Honrath et al.*, 2004], often with enhancements in CO and ozone that have been attributed to boreal fire impacts [*Lapina et al.*, 2006]. The advantage of PICO-NARE compared to measurement locations on the continent is the remote distance from source locations allowing the sampling of chemically well processed air masses.

CO at PICO-NARE was measured using a non-dispersive infrared absorption instrument (Thermo Environmental, Inc., Model 48C-TL) modified as described by *Parrish et al.* [1994]. O<sub>3</sub> was measured with a commercial ultraviolet absorption instrument (Thermo Environmental Instruments Inc., Franklin, Massachusetts, Model 49C). Data are available as 1-minute averages. For the 2-hour averages used in this study the precision for CO is estimated to be better than 9 ppbv and for O<sub>3</sub> better than 1 ppbv. For a description of the station and the measurement techniques we refer to *Honrath et al.* [2004] and *Owen et al.* [2006].

## 4.2 Model-Observation Comparison at PICO-NARE

For comparing the model simulations with the observations at PICO-NARE, the observations have been averaged in time to match the 2-hour window of the simulations, and the model data have then been linearly interpolated to the location and pressure level of the observations. Due to the coarse model resolution, the simulations do not resolve upslope events occurring at the mountain site. Observations potentially affected by upslope flow were small during summer 2004. We identified these periods as described by *Kleissl et al.* [2006] [The occurrence of upslope flows at the Pico mountain-top observatory: a case study of orographic flows on a small, volcanic island, submitted to *J. Geophys. Res.*] and omitted them from the analysis.

Figure 3 shows the time series for modeled and measured CO and O<sub>3</sub> at PICO-NARE. In addition to results from the *BB* model simulations, we also include results from the *noBB* simulation to emphasize the impact of the Alaskan/Canadian wildfires. For clarity, we reduced the temporal resolution in the graphs to daily average values, however, our analysis refers to the 2-hour average values. A detailed analysis of PICO-NARE 30-minute observations in the 2004 fire season is provided by *Val Martin et al.* [Significant Enhancement of Nitrogen Oxides, Black Carbon, and Ozone in the North Atlantic Lower Free Troposphere Resulting from North American Boreal Wildfires, submitted to *J. Geophys. Res.* (hereinafter *Val Martin et al.*, submitted)]. As can be seen, the model closely matches the observed temporal variability, and also captures the magnitudes fairly well. The mean bias between modeled and observed mixing ratios is  $-3\pm 16$  ppbv for CO and  $6\pm 12$  ppbv for O<sub>3</sub>. The corresponding biases for the simulation without fire emissions are  $-12\pm 19$  ppbv for CO and  $4\pm 12$  ppbv for O<sub>3</sub>, respectively. Daily CO fire tracers in the

model estimate a typical transport time on the order of 1–2 weeks for biomass burning plumes reaching PICO-NARE.

The time series for CO from the simulations *BB* and *noBB* indicate a clear impact from the fires at PICO-NARE throughout the months of July and August with the most extreme period from the end of July to mid-August. This is a combination of the most intense fire activity occurring in mid to end of July [Pfister *et al.*, 2005] and the transport time of 1–2 weeks. The period from July 22–24 had the highest half-hour average CO levels yet recorded at the PICO-NARE station [Val Martin *et al.*, submitted]. The impact of the fires on the ozone concentrations is less pronounced, but differences between *BB* and *noBB* of up to 10 ppbv are evident during some of the intense episodes. The difference in CO and O<sub>3</sub> concentrations between the *noBB* and the *BBsrf* simulations gives an average enhancement due to the fires of 8 ppbv (8%) for CO and 2 ppbv (4%) for O<sub>3</sub>.

The correlation between the CO mixing ratios from the simulation *BBsrf* and the observations is  $r=0.64$  compared to a correlation of  $r=0.48$  between *noBB* and the observations. During times of intense biomass burning impact, the *noBB* run actually shows slight enhancement in the CO concentrations as well, indicating that these outflow events transported pollution from the fires together with elevated pollution from likely North American anthropogenic sources.

The correlation between the measured and modeled O<sub>3</sub> is  $r=0.51$  for the simulation *noBB* and increases only slightly for the *BB* runs ( $r=0.54$ ), an indication of the less pronounced or more complex [Val Martin *et al.*, submitted] effect of the fires on the O<sub>3</sub> burden compared to the CO burden. While the model is picking up the higher ozone values

moderately well, neither the *BB* nor the *noBB* simulations capture the low end of the observed O<sub>3</sub> concentrations. This is likely due to the positive ozone bias in the model over the US, thus an overestimate of North American outflow of ozone and to an overestimate in the modeled ozone mixing ratio of maritime background air. In agreement with the conclusions drawn from the model evaluation in Section 3 it cannot be stated if either *BBsrf* or *BBvert* results in better agreement with the observations. Unless otherwise mentioned, we will focus in the following analysis on results for *BBsrf*.

## 5 Discussion

Assuming a linear relationship between CO emissions and net ozone production, the relationship between tropospheric CO and O<sub>3</sub> concentrations might be used as an estimate for the net ozone production in regional plumes [Parrish *et al.*, 1993; Forster *et al.*, 2001]. The enhancement ratio  $\Delta O_3/\Delta CO$  is defined as the difference between the ozone concentrations in a polluted air mass from that of background air, normalized by the excess mixing ratio of CO. In the case of biomass burning plumes, the background defines concentrations of CO and O<sub>3</sub> not linked to the fire emissions.

The change in the Northern Hemispheric net ozone production rate due to the fires, calculated by differencing net ozone production rates in the *BB* and the *noBB* simulation, is estimated as 6 Tg O<sub>3</sub> for June through August, a contribution of 3% to the Northern Hemispheric budget. Normalizing by the total CO emissions for this time period (30±5 Tg CO) yields a global average enhancement ratio for the fires in Alaska and Canada of 0.12 ppbv/ppbv. In the following Sections we examine the feasibility of estimating the ozone production of North American boreal fires by using enhancement ratios based on observed and modeled mixing ratios of CO and ozone at PICO-NARE.

### 5.1 Determining the Enhancement Ratio from CO and O<sub>3</sub> Observations

There are two common ways to calculate  $\Delta O_3/\Delta CO$ . The first, in the following referred to as the “scatter technique” determines the enhancement ratio from the slope of the linear fit of O<sub>3</sub> versus CO mixing ratios [Parrish *et al.*, 1993]. The second, defined “enhancement technique” infers “background” concentrations of CO and O<sub>3</sub> from air

masses not affected by the considered pollution source (in our case the wildfires in Alaska and Canada) and calculates the corresponding excess mixing ratios by subtracting background concentrations from total concentrations. Both methods are discussed in the following.

### 5.1.1 Scatter Technique

This technique has been applied in Figure 4 showing CO-O<sub>3</sub> scatter plots for observed and modeled concentrations at PICO-NARE. The data were grouped into air masses with varying biomass burning impact by using the magnitude of the observed CO mixing ratio as the threshold. Studies by *Honrath et al.* [2004] and *Lapina et al.* [2006] show that periods of extreme summertime CO concentrations frequently coincide with airflow from Northern latitudes transporting pollution from wildfires in Siberia, Alaska and Canada to PICO-NARE. To allow comparison with the observations, we applied two methods to the model data: 1) we used a threshold derived from the simulated CO, and 2) we used the relative contribution of the fire tracer *CO<sub>f</sub>*. The second method gives in some sense the true solution, as it is not impacted by sources of high CO other than the wildfires. The thresholds were chosen in a way that the number of data points was roughly equal in the different subsets. The coarse spatial resolution in the model results in a more pronounced dilution of biomass burning plumes and this explains the smaller threshold in total CO applied to the subset of high intense plumes in the model compared to the observations.

The fitting technique applied is a reduced major axis reduction (RMA). It uses the geometric mean of the slopes of the standard linear regression of *y* versus *x* and of *x* versus *y* [*Draper and Smith*, 1998] thus taking into account the variability in both

abscissa and ordinate. The mean slope and the corresponding standard deviation are specified in Figure 4.

The scatter in the data and the uncertainties in the slopes are explained by the mixture of different air masses, variability in the background CO and O<sub>3</sub> levels, and differing pathways and photochemical ages in the sampled plumes. The slopes are also somewhat dependent on the fitting technique applied. The calculated  $\Delta\text{O}_3/\Delta\text{CO}$  is independent of air mass age if the tracers used have similar lifetimes or have lifetimes much longer than the transport time, but this assumption is not entirely fulfilled in the case of CO and O<sub>3</sub>. However, in a statistical sense, a clear distinction between the different types of air masses is evident with the smallest ozone enhancements per unit CO for the most intense plumes in both model and data. In general, the features in the model data (Figure 4b) match the features in the observations (Figure 4a). However, the model does not capture the measured  $\Delta\text{O}_3/\Delta\text{CO}$  due to the impact of mixing in the model. As a result, the calculated slope has a rather large value with, at the same time, a high uncertainty. Applying the ratio  $\text{CO}_f/\text{CO}$  as a selection criteria instead (Figure 4c) we achieved a clearly stricter separation of the fire impact for the modeled plumes. The slope calculated for the most biomass burning impacted subset is then  $0.44\pm 0.08$  with a correlation of  $r=0.54$  instead of a slope of  $0.77\pm 0.57$  and a correlation of  $r=0.28$  when applying total CO mixing ratios as threshold. This slope is still higher than the observed one and this is likely due to more strongly diluted plumes in the model resulting from the coarse spatial resolution. As will be shown in Section 5.2, the selection of more intense model fire plumes reduces the estimated slope.

The generally higher slopes for air masses least impacted by biomass burning sources (defined as “non-fire plumes” here and characterized strongly by anthropogenic pollution sources) compared to those more strongly impacted by the wildfires is consistent with earlier studies and have been explained by a lower NO<sub>x</sub>:CO emission ratio in boreal fires relative to urban and industrial sources [Andreae et al., 1994]. In Figure 4c we include results from a simulation where the NO<sub>x</sub>:CO emission ratio for the wildfire emissions in the model was increased by a factor of 10 to match the emission ratio of anthropogenic sources. The pronounced difference between air masses with weak and with strong biomass burning impact is diminished in this case supporting the hypothesis that the difference between ozone production of anthropogenic and biomass burning plumes can largely be explained by a difference in NO<sub>x</sub>:CO emission ratios.

It is evident from Figure 4 that the limitations used in the selection of biomass burning impacted air masses and the degree of mixing in the considered air masses have an effect on the calculation of  $\Delta O_3/\Delta CO$ . The observed and modeled correlations also indicate that the enhancement ratio decreases the more strict the selection criteria applied are, and this dependence will be looked into more closely in Section 5.2.

### **5.1.2 Enhancement Technique**

The enhancement technique requires knowledge of the background concentrations, and large uncertainties might be introduced if the background and its variability are not well enough known. For modeling studies, however, the variability in background concentrations can be determined accurately from a simulation where the considered emission source is omitted.

Figure 5 shows observed and modeled excess mixing ratios of O<sub>3</sub> versus CO for the air mass separation applied earlier. For Figures 5a and 5b we estimated the background by averaging CO and O<sub>3</sub> mixing ratios over the subset of non-fire impacted air flow, which explains the existence of negative excess mixing ratios in this subset of data. For the observations the derived background values are 82 ppbv for CO and 37 ppbv for ozone; for the model data we obtain 81 ppbv for CO and 45 ppbv for O<sub>3</sub>. The derived slopes for the air masses impacted by biomass burning are nearly identical to the values derived from the scatter technique showing that the background value we assumed in the enhancement technique is similar to the one implied in the scatter technique. The difference in the slopes for Figures 5a and 5b suggests this method is also sensitive to the amount of mixing.

Figure 5c shows modeled slopes when the background is estimated from the simulation without fire emissions. This in some sense is the result one would obtain assuming perfect data, that is the excess mixing ratios of CO and O<sub>3</sub> are precisely known. For each data point in the *BBsurf* simulation an according background value is derived from the *noBB* run, thus the temporal variability in the background is accounted for. The standard deviation of the background mixing ratios as determined from the *noBB* simulation is on the order of 5 ppbv for the biomass burning plumes. Compared to the scatter technique and the enhancement technique with a constant background, the excess mixing ratios derived with this technique have a clearly higher correlation and are much less sensitive to the selection of the air mass.  $\Delta\text{O}_3/\Delta\text{CO}$  for the biomass burning plumes at PICO-NARE derived from this technique is 0.28 ppbv/ppbv when the air masses are filtered for the points most impacted by biomass burning, and 0.23 ppbv/ppbv for all data points.

These values are lower than those calculated earlier for the model data and match the observed  $\Delta\text{O}_3/\Delta\text{CO}$ . This concludes that the modeled fire plumes are more diluted compared to observed plumes because of the coarse model resolution, and still carry characteristics of non-fire related pollution. This impact only cancels out by considering the contribution of time-varying non-fire related background air. When the sensitivity to model mixing is removed, the model captures the observed enhancement ratio.

Thus, provided accurate information about the variability in the background levels is available, the enhancement technique allows a more accurate determination of  $\Delta\text{O}_3/\Delta\text{CO}$  than the scatter technique. The same technique applied to the model simulation in which the  $\text{NO}_x$  fire emissions were increased by a factor of 10 yields slopes on the order of 0.8, i.e. close to the enhancement ratio estimated for anthropogenic sources.

## 5.2 Enhancement Ratios and Ozone Production

We used the model data to test the sensitivity of  $\Delta\text{O}_3/\Delta\text{CO}$  derived with both the scatter and the enhancement techniques to the degree to which air masses are impacted by biomass burning. For the enhancement technique the background was derived from the *noBB* simulation. Figure 6 shows  $\Delta\text{O}_3/\Delta\text{CO}$  as a function of the magnitude of biomass burning impact indicated by selecting air masses based on a lower limit of the fraction of *CO<sub>f</sub>* to total CO. The enhancement technique shows a weak dependence on the selected air masses and the variations seen reflect the variability in ozone production in biomass burning plumes due to changes in ozone chemistry, transport pathways and times, and a combination of these or more processes. The average  $\Delta\text{O}_3/\Delta\text{CO}$  is calculated as 0.25 ppbv/ppbv for *BBsrf* and a slightly higher value, 0.27 ppbv/ppbv, is calculated for

*BBvert*. This value is close to  $\Delta O_3/\Delta CO$  derived from the observations when intense plumes are selected only (Figure 4).

Our values for  $\Delta O_3/\Delta CO$  are in the range of values found in the literature. *Mauzerall et al.* [1996] calculated enhancement ratios for aged boreal fire plumes on the order of  $0.1 \pm 0.2$  ppbv/ppbv. A value of 0.1 ppbv/ppbv was encountered during SOS-95 by *Wotawa and Trainer* [2000] and similar values during ABLE-3 for Alaska fires [*Jacob et al.*, 1992]. *McKeen et al.* [2002] report enhancement ratios of 0.17 ppbv/ppbv. Higher averaged enhancement ratios are estimated by *Bertschi and Jaffe* [2005] and *Honrath et al.* [2004] for highly aged boreal fire plumes: 0.4 ppbv/ppbv and 0.7 ppbv/ppbv, respectively.

In the case of the scatter technique it is evident that  $\Delta O_3/\Delta CO$  is higher for the weakly impacted plumes due to the mixing of the biomass burning impact with the impact of other pollution sources. As mentioned earlier, during times of intense fire plumes, increased pollution was also transported to PICO-NARE (Figure 3). The average  $O_3$  concentration for the *noBB* simulation is  $44 \pm 9$  ppbv for  $CO_f/CO < 0.01$ , but  $47 \pm 5$  ppbv and  $47 \pm 4$  ppbv for  $CO_f/CO > 0.1$  and  $CO_f/CO > 0.2$ , respectively. Corresponding CO concentrations are  $77 \pm 8$  ppbv,  $84 \pm 6$  ppbv, and  $82 \pm 6$  ppbv. When air masses with at least 20% biomass burning impact are selected, the slopes calculated with the two different techniques approaches a similar range. However, towards stricter limitations the number of data points is small and the fitting technique is less reliable.

By using  $\Delta O_3/\Delta CO = 0.25$  ppbv/ppbv as derived from the enhancement technique, an approximation for the total ozone produced from the fires can be made [*Parrish et al.*, 1993; *Mauzerall et al.*, 1996]. With  $30 \pm 5$  Tg CO emitted by the fires from June through

August as stated by *Pfister et al.* [2005], an ozone production of 10.7–15 Tg O<sub>3</sub> is estimated for the same time period.

This value is larger than the Northern Hemispheric net chemical production rate of 6 Tg O<sub>3</sub> in the model as mentioned earlier. The discrepancy can be explained in that  $\Delta\text{O}_3/\Delta\text{CO}$  at the location of PICO-NARE is not representative for the total net change in ozone, but rather for the net ozone production rate covering the region from the source location to the Azores. Close to the source region net chemical production of fire-related ozone dominates, while further downwind from the source (e.g. Europe and Asia) net chemical loss dominates. The modeled net ozone production calculated over a region representative for air masses reaching PICO-NARE (stretching from 180W to 20W and from 40N to 70N) is 9 Tg O<sub>3</sub> for *BBsrf* and 11 Tg O<sub>3</sub> for *BBvert*, i.e. in the range of the estimate based on  $\Delta\text{O}_3/\Delta\text{CO}$ . These results demonstrate that the measurements and model simulations at the location of PICO-NARE being representative of aged biomass burning plumes indeed give a good measure of the ozone production of fires in North America. Differences between the  $\Delta\text{O}_3/\Delta\text{CO}$  based estimate and the model calculated production are explained by uncertainties in the calculation of the slopes and differing pathways and chemical ages for plumes reaching PICO-NARE.

As mentioned earlier, our model simulations not only include a CO fire tracer, but also an ozone fire tracer  $\text{O}_3^{\text{NO}_x}$  that tracks the amount of ozone produced from the NO<sub>x</sub> fire emissions. One might assume that the global net ozone production for this tracer equals the amount derived when subtracting results for simulations with and without fire emissions as has been done above (6 Tg O<sub>3</sub>). However, the net ozone production rate for the Northern Hemisphere calculated from the ozone fire tracer is higher, close to 9 Tg O<sub>3</sub>.

The reasons for this are due to the non-linearity in ozone chemistry and are explored in the following Section.

### 5.3 Changes in the Ozone Chemistry due to Fire Emissions

In Figure 7 we show correlations between the model CO and O<sub>3</sub> fire tracers and the difference in O<sub>3</sub> and CO mixing ratios from *BBsrf* and *noBB* simulations defined as  $dO_3$  and  $dCO$ , respectively. As can be seen, the correlation for CO is close to the 1:1 line, but for ozone the mixing ratios of  $O_3^{NO_x}$  are clearly larger compared to  $dO_3$  indicating that ozone production related to the fires must have been offset by an increased loss of ozone.

To explore the mechanisms behind the ozone production from the fire emissions, we compared ozone concentrations, production and loss terms in the model for the simulations *BBsrf* and *noBB*. The data set has been split into three groups of varying fire impact determined by the ratio  $CO_f/CO$ . Statistics for the individual subsets are plotted in Figure 8. The maps (Figure 8a) denote the geographical coverage of the selected data with red indicating a high, and blue a low, concentration of data points. The most intense plumes are concentrated near the source location, but plumes of high fire impact can also be seen all the way to Europe. The high intensity plumes are mostly located near the surface (Figure 8b) as expected when the emissions are released at the lowest model level. With time, atmospheric transport and convection spread plumes over a larger altitude range.

Figure 8c shows that ozone levels without fire emissions ( $O_{3noBB}$ ) are mostly below 40 ppbv over the source regions, i.e. the fires occurred in an area of low ozone concentrations. The additional NO<sub>x</sub> from the fires causes a shift in the distribution of

ozone concentrations towards higher values. The effect is most pronounced over the source region, but a slight positive shift is also evident for the subset of least impacted plumes.

The increase in ozone is caused by a strong net production of the fire tracer  $O_3^{NOx}$  in the most impacted plumes with the magnitude decreasing with decreasing plume intensity. This is shown in Figure 8d where we illustrate histograms for the  $O_3^{NOx}$  net chemical production. Even though the strongest production takes place close to the source region, continuing production is also evident in regions further downwind from the source. For the subset of least impacted plumes (and most aged plumes), there are a significant number of data points with net chemical loss of  $O_3^{NOx}$ .

Figures 8e to 8g show the changes to background ozone levels when fire emissions are injected into the system. Figure 8e denotes the distribution for production of  $O_3noBB$  and of background ozone with fire emissions; the latter defined as  $O_3B$ .  $O_3B$  is calculated by subtracting the ozone fire tracer from the total ozone. The production of  $O_3B$  is less than the production of  $O_3noBB$ . Thus, by adding fire emissions to the system, the production of background ozone is reduced in the simulations. This is due to a decrease in peroxy radical concentrations (not shown here). Changes are most pronounced over the source region, but differences are also evident in less impacted plumes.

In addition to a reduced production of  $O_3B$ , the loss of  $O_3B$  is increased over that of  $O_3noBB$ , reflected in a reduction in the chemical lifetime (Figure 8f). The reduced production and increased loss of background ozone result in lower concentrations of  $O_3B$  compared to  $O_3noBB$ . In Figure 8g we show the corresponding frequency distributions for  $O_3^{NOx}$ ,  $O_3B$  and  $dO_3$ . When compared to Figure 8c we see that over the source region

$O_3B$  has on average ~80% smaller values compared to  $O_3noBB$  and most of the ozone present is in the form of  $O_3^{NOx}$ , i.e. ozone due to the  $NO_x$  fire emissions.

The strong reduction of background ozone levels when fire emissions are included explains why concentrations of  $O_3^{NOx}$  are larger than the difference in ozone concentrations between runs with and without fire emissions. In contrast, the CO chemistry has a first-order linearity, thus the concentrations of the fire tracer  $CO_f$  are close to the difference of CO concentrations simulated with and without fire emissions (Figure 7). However, the fires also impacted background levels of atmospheric CO to some extent. The high VOC and CO emissions from the fires result in a reduction in average OH concentrations. This in turn reduces the rate of oxidation of CO and results in increased background CO levels. This increase has been estimated in the model by comparing the background CO with fire emissions (calculated by subtracting  $CO_f$  from total CO concentrations in  $BBsrf$ ) to the CO field without fire emissions. For the Northern Hemisphere we calculate an increase in the burden of background CO of up to 1 Tg CO.

#### **5.4 Impact of Alaska/Canada Wildfires on the Ozone Budget**

Finally, using the model results, we examine how increases in the CO and ozone concentration fields related to the wildfires affected the Northern Hemispheric and the regional trace gas budgets. In Figure 9 we show the time series for the modeled Northern Hemispheric CO and ozone burden (surface – 300 hPa) and the changes related to the emissions from the fires. The change in the CO burden reaches close to 10% around the end of July. The corresponding changes in the ozone burden are on the order of up to 4%. On average, the Northern Hemispheric CO and  $O_3$  burden during the summer 2004 were increased due to emissions by the fires by 4–5% and 2%, respectively.

As expected, the largest changes in the atmospheric burden occurred over Alaska and Canada (50–70N, 180E–60W) with an average increase in the ozone burden of 7–9% for the altitude range surface–300 hPa, and 11–12% for the range surface–800 hPa. For comparison, over the altitude range up to 300 hPa, this is slightly smaller than the estimated contribution of stratospheric ozone (11%) in the model, but for the range up to 800 hPa exceeds the contribution of stratospheric ozone (3%).

Due to the transport of ozone and ozone precursors, effects from the fires are also expected far downwind of the source location. Over Europe (35–70N, 20W–20E) we estimate a contribution of ozone from the fires of up to 10% around the end of July for the surface–300 hPa range and up to 8% for the range surface–800 hPa. Averaged over the summer, the contributions are on the order of 3% for both altitude ranges considered. These results show that even though the fires had a rather small contribution to the large-scale hemispheric budget of ozone, over certain regions and altitudes, even far downwind from the source itself, the impact is significant.

## 6 Conclusion

Controversies exist in the understanding of the importance of ozone production from boreal forest fires. By combining the information from observations and modeling studies we have determined the amount of ozone produced from the wildfires in Alaska and Canada in summer 2004. The modeled CO and ozone fields have been evaluated by comparison with a comprehensive set of aircraft measurements taken during the ICARTT campaign.

In analyzing the ozone production from North American boreal fires we used measured and modeled CO and ozone mixing ratios at the PICO-NARE station in the Azores. The results show that the enhancement ratio  $\Delta O_3/\Delta CO$ , defined as the increase in ozone per unit increase in CO, derived from observed and modeled concentrations at PICO-NARE is a good measure for the ozone production from the Alaska and Canada fires. However, we also show that this measure can be very sensitive to the selected air masses. Our analysis yields enhancement ratios of 0.25 ppbv/ppbv for aged plumes of Alaskan and Canadian wildfires, which is in the range of values found in the literature. The enhancement ratio found for boreal biomass burning plumes is about a factor of 3–4 smaller than that of anthropogenic plumes. A model sensitivity study indicates that this difference is mostly due to differences in the  $NO_x:CO$  emission ratios between these sources.

The modeled total net ozone production from the boreal fires in Alaska and Canada in the summer of 2004 in the model is estimated as 6 Tg  $O_3$  which gives a contribution of about 3% to the Northern Hemispheric budget. Considering only a region spanning from the

source to the Azores, a net chemical production of 9–11 Tg O<sub>3</sub> is calculated in the model. This is in agreement with the estimate derived from enhancement ratios based on model simulations and observations at PICO-NARE (10.7–15 Tg O<sub>3</sub>). Large increases in the ozone burden are observed downwind of the fires due to transport of ozone produced near the fires as well as due to continuing ozone production in the fire plumes. Modeling studies show that the increase in the atmospheric burden of ozone is a combination of a strong ozone production due to precursors emitted by the fires, and an increased destruction of ozone background levels resulting from reduced peroxy radical concentrations.

While the availability of satellite measurements of tropospheric CO concentrations allows putting constraints on the CO emissions, uncertainties remain in how to constrain the emissions of NO<sub>x</sub> and VOCs resulting in uncertainties in the estimated ozone production. Another unknown is the emissions injection height of the fires. Even though the impact was small in the specific case we looked at, in other regions, seasons or under different synoptic conditions sensitivities might become more pronounced.

The results of this study indicate that fires in the boreal region can have a significant impact on the ozone production over large parts of the Northern Hemisphere. We focused our investigations on the wildfires in Canada and Alaska from summer 2004, that have been a record for this region, but comparable or even larger impacts might occur from fires in Siberia. With climate change and the possibility of increased fire activity in the Northern latitudes as a result of more frequent and/or more severe droughts and increased direct human impact [Mollicone *et al.*, 2006], ozone production from boreal fires might even gain in importance in the future.

## Acknowledgements

The authors greatly appreciate the helpful comments provided by Brian Ridley and John Orlando. Measurements at PICO-NARE are funded by NOAA Office of Global Programs grants NA16GP1658, NA86GP0325, NA03OAR4310002, and NSF grants ATM0215843 and INT-0110397. The work was supported by NASA grants EOS/03-0601-0145 and NNG04GA459. NCAR is operated by the University Corporation of Atmospheric Research under sponsorship of the National Science Foundation.

## References

- Andreae, M.O. and P. Merlet (2001), Emissions from trace gases and aerosols from biomass burning, *Global Biogeochem. Cycles*, 15, 955-966.
- Andreae, M. O., B. E. Anderson, D. R. Blake, J. D. Bradshaw, J. E. Collins, G. L. Gregory, G. W. Sachse, M. C. Shipham (1994), Influence of plumes from biomass burning on atmospheric chemistry over the equatorial and tropical South Atlantic during CITE 3, *J. Geophys. Res.*, 99(D6), 12793-12808, doi:10.1029/94JD00263.
- Averill, C., D. Mazzone, J. Logan, L. Tong, D. Diner, Q. Li (2005), Combining MISR and MODIS Data to Automatically Catalog Smoke Plumes in North America. *The Earth Observer*, 17 (6), pp. 11-12, Nov-Dec 2005.
- Avery, M. A., Plant, J. V. and C. H. Hudgins, FASTOZ: An accurate, fast-response in situ ozone measurement system for aircraft campaigns, *J. Oceanic and Atmos. Tech.*, submitted.
- Bertschi, I.T. and D.A. Jaffe (2005), Long-Range Transport of ozone, carbon monoxide, and aerosols to the NE Pacific troposphere during the summer of 2003: Observations of smoke plumes from Asian boreal fires, *J. Geophys. Res.*, 110, doi:10.1029/2004JD005135.
- Browell E.V. et al., Large scale ozone and aerosol distributions, air mass characteristics, and ozone fluxes over the western pacific ocean in late winter/early spring (2003), *J. Geophys. Res.*, 180 (D20), doi:10.1029/2002JD003290.
- Chandra, S., J.R Ziemke, X. Tie, G. Brasseur (2004), Elevated Ozone in the Troposphere over the Atlantic and Pacific Oceans in the Northern Hemisphere, *Geophys. Res. Letters*, 31, L23201, doi:10.1029/2004GL020821.
- Draper N.R. and H. Smith (1998), Applied Regression Analysis, John Wiley, Hoboken, N.J.

- EPA, U. S. (2004), EPA Clearinghouse for inventories and emissions factors: 1999 National Emission Inventory Documentation and Data – Final Version 3.0, <http://www.epa.gov/ttn/chief/net/1999inventory.html>
- Forster, C., U. Wandinger, G. Wotawa, P. James, I. Mattis, D. Althausen, P. Simmonds, S. O'Doherty, S. G. Jennings, C. Kleefeld, J. Schneider, T. Trickl, S. Kreipl, H. Jäger, A. Stohl (2001), Transport of boreal forest fire emissions from Canada to Europe, *J. Geophys. Res.*, 106(D19), 22887-22906, 10.1029/2001JD900115.
- Gerbig, C.D., S. Schmitgen, D. Kley, A. Volz-Thomas, K. Dewey, and D. Haaks, An improved fast-response vacuum-UV resonance fluorescence CO instrument (1999), *J. Geophys. Res.*, 104 (D1), 1699-1704.
- Gerbig, C.D., et al. (1996), Fast response resonance fluorescence CO measurements aboard the C130: instrument characterization and measurements made during North Atlantic Regional Experiment 1993, *J. Geophys. Res.*, 101, 29229-29238.
- Granier, C. et al. (2004), Present and future surface emissions of atmospheric compounds, European Commission report EVK 2199900011. (Available at <http://www.aero.jussieu.fr/projet/ACCENT/POET.php>)
- Holloway, J.S., R.O. Jakoubec, D.D. Parrish, C. Gerbig, A. Volz-Thomas, S. Schmitgen, A. Fried, B. Wert, B. Henry, J.R. Drummond (2000), Airborne intercomparison of vacuum ultraviolet fluorescence and tunable laser diode absorption measurements of tropospheric carbon monoxide, *J. Geophys. Res.*, 105, 24251-24261.
- Honrath R. E., R. C. Owen, M. Val Martín, J. S. Reid, K. Lapina, P. Fialho, M. P. Dziobak, J. Kleissl, D. L. Westphal (2004), Regional and hemispheric impacts of anthropogenic and biomass burning emissions on summertime CO and O<sub>3</sub> in the North Atlantic lower free troposphere, *J. Geophys. Res.*, 109, D24310, doi:10.1029/2004JD005147.
- Horowitz L. W., et al. (2003), A global simulation of tropospheric ozone and related tracers: Description and evaluation of MOZART, version 2, *J. Geophys. Res.*, 108 (D24), 4784, doi:10.1029/2002JD002853.
- Houghton, J.T., Y. Ding, D.J. Griggs, M. Noguera, P.J. van der Linden, X. Dai, K. Maskell, and C.A. Johnson (2001), Climate Change 2001: The Scientific Basis – Contribution of Working Group I to the Third Assessment Report of the Intergovernmental panel on Climate Change, Cambridge Univ. Press, New York.
- Jacob, D.J. et al. (1992), Summertime Photochemistry of the Troposphere at High Northern Latitudes, *J. Geophys. Res.*, 97 (D15), 16,421-16,431.
- Kistler, R., E. Kalnay, W. Collins, S. Saha, G. White, J. Woollen, M. Chelliah, W. Ebisuzaki, M. Kanamitsu, V. Kousky, H. van den Dool, R. Jenne, and M. Fiorino, 2001: The NCEP-NCAR 50-Year Reanalysis: Monthly Means CD-ROM and Documentation. *Bull. Amer. Meteor. Soc.*, 82, 247-268.
- Lamarque J.-F., P. Hess, L. Emmons, L. Buja, W. Washington, C. Granier (2005), Tropospheric ozone evolution between 1890 and 1990, *J. Geophys. Res.*, 110, D08304, doi:10.1029/2004JD005537.

- Lapina, K., R. E. Honrath, R. C. Owen, M. Val Martin, and G. Pfister (2006), Evidence of significant large-scale impacts of boreal fires on ozone levels in the midlatitude Northern Hemisphere free troposphere, *Geophys. Res. Lett.*, 33, L10815, doi:10.1029/2006GL025878.
- Marenco, A. et al. (1998), Measurement of ozone and water vapour by Airbus in-service aircraft: The MOZAIC airborne program, an overview, *J. Geophys. Res.*, 103, 25,631-25,642.
- Mauzerall, D.L., D.J. Jacob, S.-M. Fan, J.D. Bradshaw, G.L. Gregory, G.W. Sachse, D.R. Blake (1996), Origin of tropospheric ozone at remote high northern latitudes in summer, *J. Geophys. Res.*, 101 (D2), 4175-4188.
- Mollicone, D., H.D. Eva, F. Achard (2006), Human Role in Russian wildfires, *Nature*, 440, 436-437.
- McKeen S. A., G. Wotawa, D. D. Parrish, J. S. Holloway, M. P. Buhr, G. Hübler, F. C. Fehsenfeld, J. F. Meagher (2002), Ozone production from Canadian wildfires during June and July of 1995, *J. Geophys. Res.*, 107 (D14), doi:10.1029/2001JD000697.
- Nedelec, P., J.P. Cammas, V. Thouret, G. Athier, J.M. Cousin, C. Legrand, C. Abonnel, F. Lecoœur, G. Cayez, M. Marizy (2003), An improved infra-red carbon monoxide analyser for routine measurements aboard commercial Airbus aircraft: Technical validation and first scientific results of the MOZAIC program, *Atmos. Chem. Phys.*, 3, 1551-1564.
- Owen, R.C., O.R. Cooper, A. Stohl, R.E. Honrath (2006), An analysis of transport mechanisms of North American emissions to the central North Atlantic, *J. Geophys. Res.*, in press.
- Parrish, D.D., J.S. Holloway, M. Trainer, P.C. Murphy, G.L. Forbes, F.C. Fehsenfeld (1993), Export of North American Ozone Pollution to the North Atlantic Ocean, *Science*, 259, 1436-1439.
- Parrish, D.D., J.S. Holloway, F.C. Fehsenfeld (1994), Routine, continuous, measurement of carbon monoxide with parts per billion precision, *Environ. Sci. Technol.*, 28, 1615-1618.
- Pfister G., P. G. Hess, L. K. Emmons, J.-F. Lamarque, C. Wiedinmyer, D. P. Edwards, G. Pétron, J. C. Gille, G. W. Sachse (2005), Quantifying CO emissions from the 2004 Alaskan wildfires using MOPITT CO data, *Geophys. Res. Lett.*, 32, L11809, doi:10.1029/2005GL022995.
- Ryerson, T. B., M. P. Buhr, G. J. Frost, P. D. Goldan, J. S. Holloway, G. Hübler, B. T. Jobson, W. C. Kuster, S. A. McKeen, D. D. Parrish, J. M. Roberts, D. T. Sueper, M. Trainer, J. Williams, F. C. Fehsenfeld (1998), Emissions lifetimes and ozone formation in power plant plumes, *J. Geophys. Res.*, 103(D17), 22,569-22,584, 10.1029/98JD01620.
- Sachse, G.W., G.F. Hill, L.O. Wade, M.G. Perry (1987), Fast-response, high precision carbon monoxide sensor using a tunable diode laser absorption technique, *J. Geophys. Res.*, 92, 2071-2081.

- Schlager, H., et al. (1997), In situ observations of air traffic emission signatures in the North Atlantic flight corridor, *J. Geophys. Res.*, 102, 10739-10750.
- Wofsy, S. C., G. W. Sachse, G. L. Gregory, D. R. Blake, J. D. Bradshaw, S. T. Sandholm, H. B. Singh, J. A. Barrick, R. C. Harriss, R. W. Talbot, M. A. Shipham, E. V. Browell, D. J. Jacob, J. A. Logan (1992), Atmospheric chemistry in the arctic and subarctic: Influence of natural fires, industrial emissions, and stratospheric inputs, *J. Geophys. Res.*, 97(D15), 16731-16746, 10.1029/92JD00622.
- Wotawa, G. and M. Trainer (2000), The influence of Canadian forest fires on pollutant concentrations in the United States, *Science*, 288, 324-328.
- Yokelson R. J., I. T. Bertschi, T. J. Christian, P. V. Hobbs, D. E. Ward, W. M. Hao (2003), Trace gas measurements in nascent, aged, and cloud-processed smoke from African savanna fires by airborne Fourier transform infrared spectroscopy (AFTIR), *J. Geophys. Res.*, 108 (D13), 8478, doi:10.1029/2002JD002322.

<b>Aircraft</b>	<b>Species</b>	<b>Instrument</b>	<b>Reference</b>
NASA-DC8	CO	Tunable Diode Laser Absorption	<i>Sachse et al., 1987</i>
	O <sub>3</sub>	NO Chemiluminescence	<i>Avery et al., submitted</i>
	O <sub>3</sub>	Airborne Differential Absorption Lidar (DIAL)	<i>Browell et al., 2003</i>
NOAA-P3	CO	VUV CO Fluorescence	<i>Holloway et al., 2000</i>
	O <sub>3</sub>	NO Chemiluminescence	<i>Ryerson et al. (1998)</i>
UK BAE146	CO	VUV Resonance Fluorescence	<i>Gerbig et al., 1999</i>
	O <sub>3</sub>	UV Absorption	<i>Thermo Electron Co. Model 49</i>
DLR Falcon	CO	VUV Fluorescence	<i>Gerbig et al., 1996</i>
	O <sub>3</sub>	UV Absorption	<i>Schlager et al., 1999</i>
MOZAIC	CO	Improved IR Correlation	<i>Nedelec et al., 2003</i>
	O <sub>3</sub>	UV Absorption	<i>Marenco et al., 1998</i>

Table 1: List of aircraft measurements included in the evaluation of the model simulations. The NOAA-P3 O<sub>3</sub> instrument is a new installation, but similar to the one described in the listed reference.

	<i>BBsrf</i>	<i>BBvert</i>	<i>noBB</i>	<i>BBsrf to noBB</i>	<i>BBvert to noBB</i>	<i>BBsrf to BBvert</i>
	<i>CO (ppbv) Mean and Std. Dev.</i>			<i>CO T-test Significance</i>		
<i>DC-8</i>	119±37	117±35	106±31	< 0.01	< 0.01	0.01
<i>P-3</i>	140±41	139±41	124±39	< 0.01	< 0.01	0.07
<i>BAE146</i>	100±24	99±23	84±13	< 0.01	< 0.01	0.14
<i>Falcon</i>	110±24	108±23	85±11	< 0.01	< 0.01	0.06
<i>MOZAIC</i>	117±39	116±39	105±36	< 0.01	< 0.01	0.06
	<i>O<sub>3</sub> (ppbv) Mean and Std. Dev.</i>			<i>O<sub>3</sub> T-test Significance</i>		
<i>DC-8</i>	59±14	60±14	57±14	< 0.01	< 0.01	0.02
<i>P-3</i>	59±10	59±10	57±10	< 0.01	< 0.01	< 0.01
<i>BAE146</i>	51±14	52±15	48±12	< 0.01	< 0.01	< 0.01
<i>Falcon</i>	58±11	59±11	53±10	< 0.01	< 0.01	0.01
<i>MOZAIC</i>	62±13	63±13	60±13	< 0.01	< 0.01	< 0.01
<i>DIAL</i>	54±8	56±9	53±8	< 0.01	< 0.01	< 0.01

Table 2: Statistics over the altitude range 0-8 km for the model simulations *BBsrf*, *BBvert* and *noBB* and the platforms listed in Table 1. Mean and standard deviation for CO and O<sub>3</sub> concentrations and the significance level of the Student's T-Statistics comparing *BBsrf* to *noBB*, *BBvert* to *noBB*, and *BBsrf* to *BBvert* are shown.

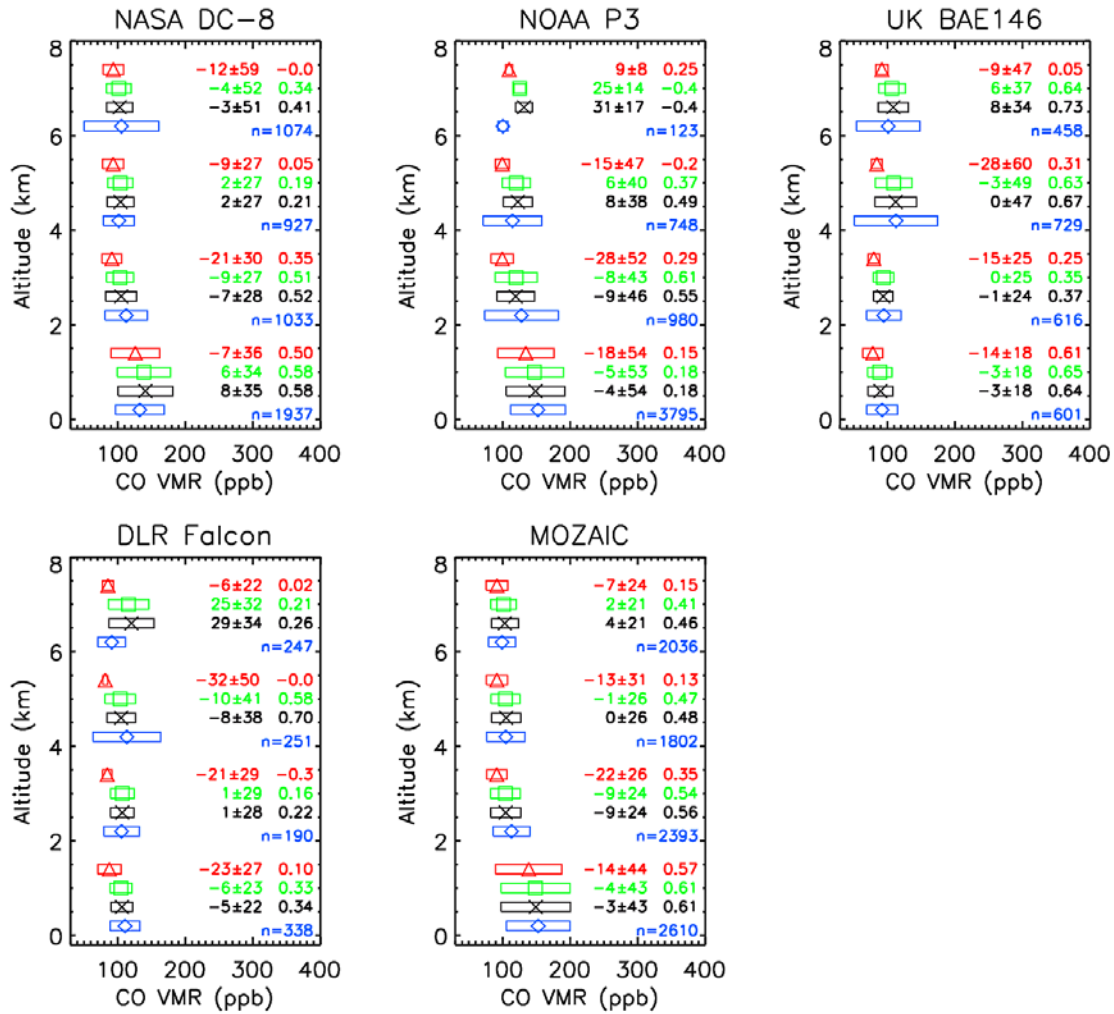


Figure 1: Model evaluation with aircraft data for CO (blue diamonds: observations, black crosses: model with fire emissions injected at surface; green squares: model simulations with fire emissions injected over 0-9 km; red triangles: no fire emissions). The mean percent bias and standard deviation (model minus measurement), correlation coefficient  $r$  and number of data points for 2-km wide altitude bins are specified.

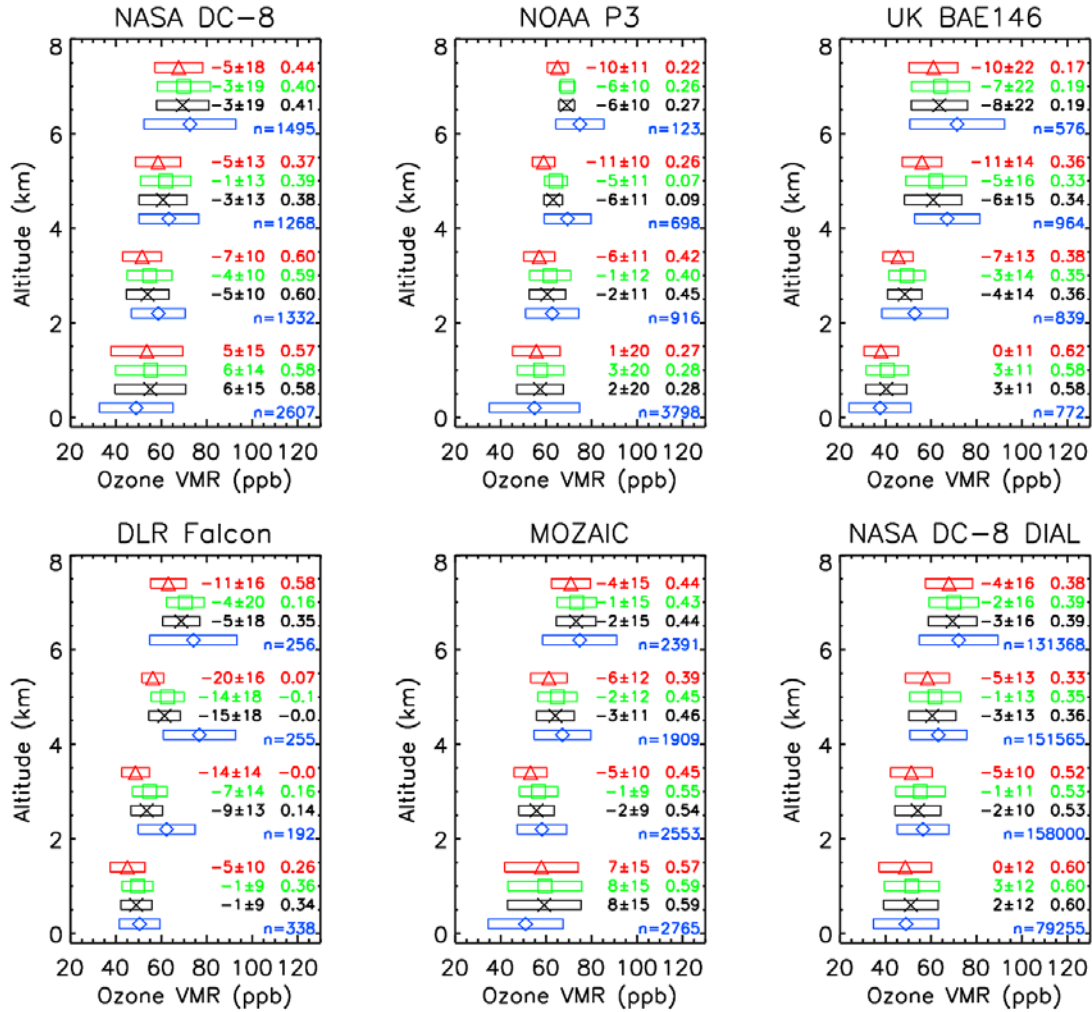


Figure 2: As Figure 1, but for ozone.

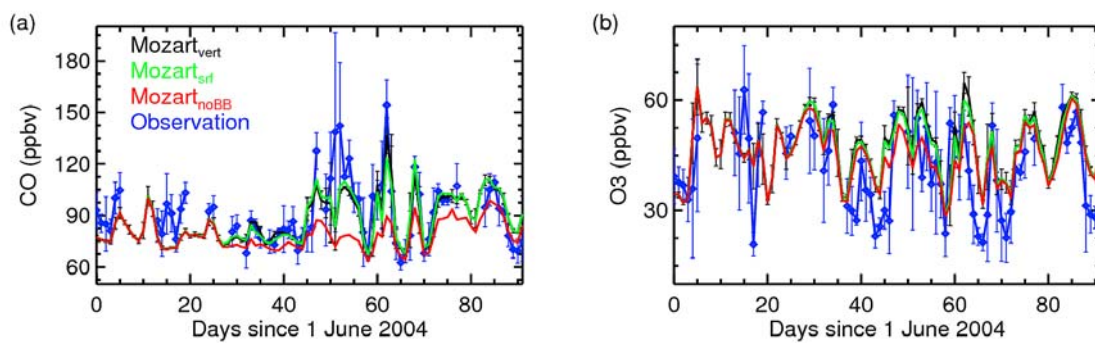


Figure 3: Measured and modeled time series of CO and O<sub>3</sub> mixing ratios at PICO-NARE (daily averages are shown).

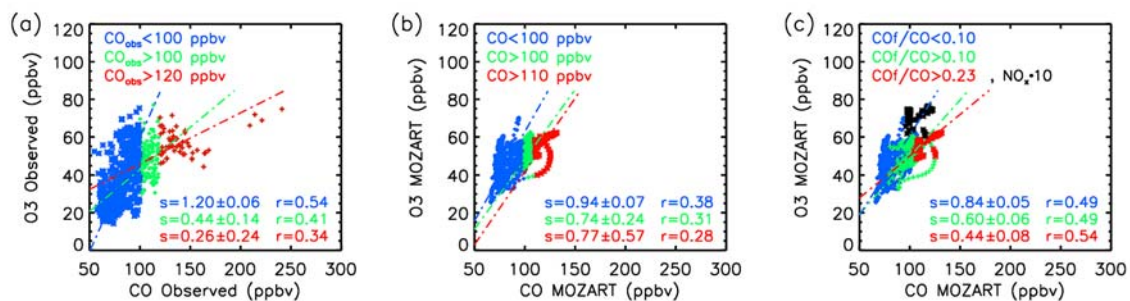


Figure 4: Observed (a) and modeled (b,c) CO-O<sub>3</sub> relationships at PICO-NARE. Air masses are separated into three groups: mostly non-fire related origin (blue), some biomass burning impact (green), pronounced biomass burning impact (red). In (c) results are also shown for a simulation where the NO<sub>x</sub> fire emissions were increased by a factor of 10.

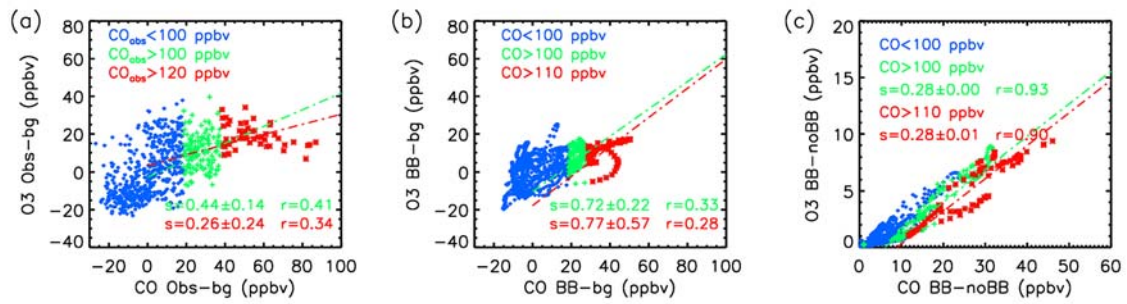


Figure 5: Observed (a) and modeled (b,c) CO-O<sub>3</sub> excess mixing ratios. In (a) and (b) a constant background is calculated from the subset of non-fire impacted airmasses, in (c) the background is derived from the *noBB* simulation.

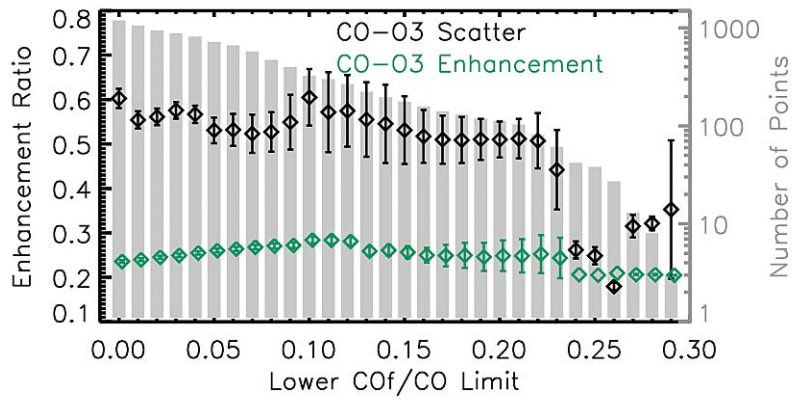


Figure 6: Enhancement Ratio (mean slope and standard deviation) determined by the scatter and the enhancement technique as a function of intensity of biomass burning influence of considered air masses. The number of selected data points is represented by the shaded area. Results for the *BBsrf* simulation.

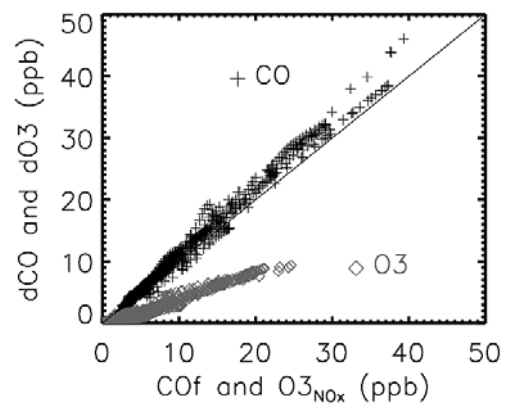


Figure 7: Correlation between the model fire tracers  $CO_f$  and  $O_3^{NO_x}$  and the difference in CO and  $O_3$  mixing ratios between the simulations  $BBsrf$  and  $noBB$  (defined as  $dCO$  and  $dO_3$ ) at PICO-NARE.

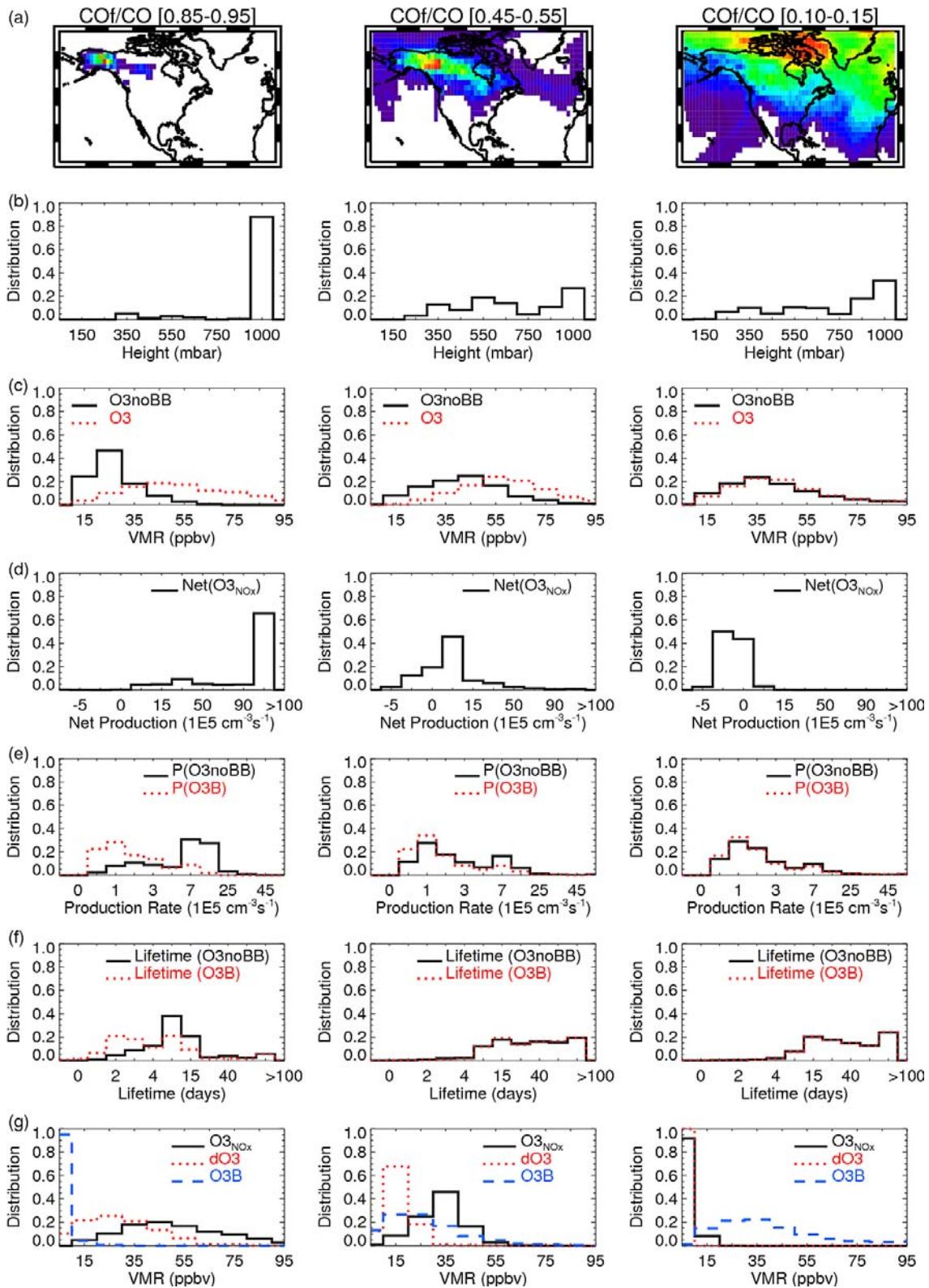


Figure 8: Statistics for ozone concentrations and ozone production and loss terms for three different subsets of fire plume intensity as characterized by the ratio of  $CO_f/CO$ . (a) Spatial distribution for selected data points. (b) Frequency distribution for the height of the selected data points (c) Frequency distribution of the volume mixing ratios  $O_3noBB$  and  $O_3$ . (d) Net ozone production rate for the fire tracer  $O_3^{NOx}$  (e) Frequency distribution of the ozone production rate for  $O_3noBB$  and  $O_3B$  (background ozone estimated by subtracting  $O_3$  and  $O_3^{NOx}$ ). (f) as (e) but for the chemical lifetime (g). Frequency distribution of the volume mixing ratios  $O_3^{NOx}$ ,  $dO_3$  and  $O_3B$ .

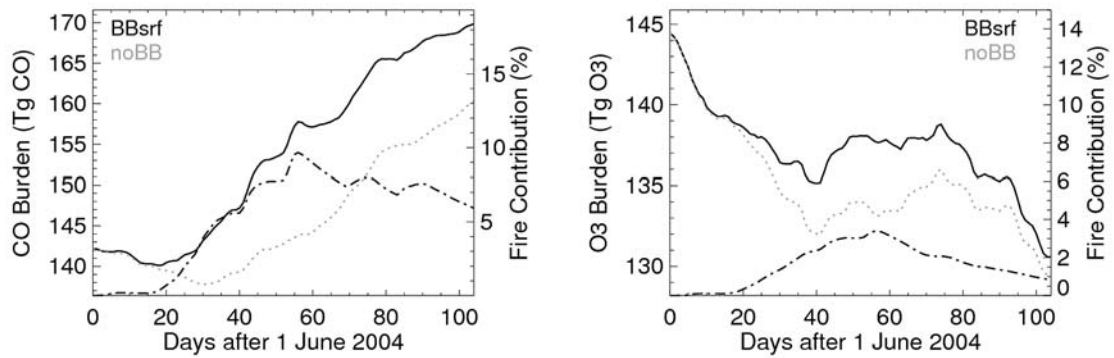


Figure 9: Northern Hemispheric burden of CO and O<sub>3</sub> for the altitude range surface-300 mbar. Model results for simulations *BBsrf* (solid line) and *noBB* (dotted line). The dash-dotted line denotes the percentage difference between simulations *BB* and *noBB* (shown on the secondary ordinate).